Channel-interaction effects on the 3p-subshell photoionization of chlorine

William R. Fielder* and Lloyd Armstrong, Jr.
Department of Physics, The Johns Hopkins University, Baltimore, Maryland 21218
(Received 7 May 1982; revised manuscript received 24 January 1983)

Photoionization cross sections and photoelectron angular distributions (asymmetry parameters) are obtained for 3p-subshell ionization of the Cl ground state. A substantial amount of bound-state electron correlation is taken into account through use of a multiconfiguration description of the ground state and residual ionic core. Both independent-channel and coupled-channel final states are used in evaluating the length and velocity forms of the dipole transition amplitudes. In the coupled-channel case, channel interaction is included via the reaction-matrix (K-matrix) method which diagonalizes the total N-electron atomic Hamiltonian in the manifold of single-channel basis states of the model Hamiltonian. In all of the ^2D and ^2P final-state channels, the photoabsorption transition probabilities exhibit significant contributions from interchannel interaction. In determining the cross sections for any of the ^2S channels, it was necessary to include the low-lying $3s\,3p^6;^2S$ bound state because of its large Coulomb interaction with the continuum of the $3p^4\,^1D,\epsilon d;^2S$ channel. The addition of the channels which originate from a $3s\rightarrow\epsilon p$ transition into the set of interacting ^2S channels nearly cancels the effect of the $3s\,3p^6;^2S$ discrete state on the cross sections of both the $3p^4\,^1D,\epsilon d;^2S$ and $3p^4\,^1S,\epsilon s;^2S$ channels. The asymmetry parameters for the three ionic multiplets ^3P, ^1D, and ^1S all show strong channel-interaction effects. The effects of the $3s\,3p^6;^2S$ bound state and the $3s\,3p^5;^{3,1}P,\epsilon p;^2S$ channels on the ^1D and ^1S β parameters are discussed.

I. INTRODUCTION

The study of electron-correlation effects in atomic photoionization has proceeded in recent years from the now well-understood closed-shell noble-gas atoms to the less understood and more complicated open-shell systems. Of these open-shell atoms, chlorine has lately been the object of numerous theoretical investigations.[1–6] One reason for this interest in chlorine lies in the nature of its ground state: it lacks one outer electron of being the ground state of the noble gas argon, which has been studied extensively. As a number of different theories produce photoionization cross sections in good agreement with one another and with experiment for the noble gases, it is informative to compare the results of these theories when they are applied to an open-shell atom which is "almost" a noble gas.

Among the various methods used in the theoretical investigations of Cl are close coupling,[1] random-phase approximation with exchange (RPAE),[2,3] R matrix,[4] and many-body perturbation theory (MBPT),[5] all of which produce photoionization cross sections which asymptotically become similar in the region of high photon energies (greater than about 1.4 a.u.) but differ by substantial amounts near the ionic thresholds. As a result of this quantity of theoretical information, and its lack of conformity, we have undertaken another calculation of the photoionization cross sections and photoelectron angular distributions for ionization of the 3p subshell of chlorine, employing a different theoretical tool: the multiconfiguration Hartree-Fock (MCHF) method.

Until a few years ago the MCHF had not been utilized in photoabsorption studies, probably because quite sophisticated MBPT methods had been successful in determining photoionization cross sections for rare-gas atoms, leaving the impression that a technique as straightforward as the MCHF would not be appropriate. However, Swanson and Armstrong[7] demonstrated that the MCHF produced as good a description of the ground states of the noble gases as was required for obtaining accurate photoabsorption cross sections. These ground states, used in conjunction with final-state continuum wave functions constructed in a $V^{N-1}(\gamma SL)$ Hartree-Fock potential,[8] led to reasonable values of the photoionization cross sections for all the rare gases. Extending their $V^{N-1}(\gamma SL)$ potential to include multiconfiguration descriptions of the residual ion led to the $MCV^{N-1}(\gamma SL)$ potential, which permitted Swanson and Armstrong to incorporate many of the important final-state ionic-core electron-correlation effects in the noble gases. The resulting MCHF calculation[7] produced photoabsorption cross sections comparable in accuracy to those obtained with the RPAE[8] and the R matrix,[9] even though interchannel coupling in the final state was neglected. The application of these MCHF techniques to the chlorine study will be discussed in Sec. II.

Perhaps the most significant single difference between photoionization from a closed-shell rare-gas atom and photoionization from an open-shell atom, such as chlorine, is in the states of the residual ion which can be produced. For example, the $3p^5$ ground-state configuration for Ar^+ can form only the ^2P LS-coupled state. In Cl^+, on the other hand, the ground configuration is $3p^4$ which can be coupled to form ^3P, ^1D, and ^1S states. These ionic states are mixed in the presence of the photoelectron and the coupling between the resulting channels should be included in the description of the final-state wave function. Several studies of chlorine photoionization have indicated that this channel mixing is one of the most important aspects of the problem.[1,3–5]

In the present work, we made use of the reaction matrix (K matrix) to couple the final-state channels by diagonalizing the total Hamiltonian in the final state. In this approach, one obtains a basis set of final-state wave func-

tions for the various channels employing an independent-channel method. The K matrix is then used to construct final-state wave functions which are eigenfunctions of the total N-electron Hamiltonian, and which asymptotically yield the residual-ion-plus-photoelectron systems belonging to the various observed channels. The implementation of this procedure is discussed in Sec. II B.

The channel-interaction MCHF partial and total photoionization cross sections, calculated using the theoretical procedures outlined in Secs. II and III, are discussed and compared to other theoretical calculations[1-6] in Secs. IV and V. The asymmetry parameter β of the differential cross section was determined for each of the three multiplets of the ionic configuration $Cl^+ 3p^4$ in both the independent-channel and channel-interaction approximations; these results are presented in Sec. VI and compared with other recent evaluations.[2,6] Considerably more detail on all the points discussed in this paper can be found in Ref. 10.

II. STATES

In this study, we have used the MCHF to calculate the effects of correlation in the ground state of the atom, and in the low-lying states of the final ion. Additional interchannel correlation in the final state is included using the K matrix. In this section, we describe the types of correlation studied in this work.

A. Initial state

Recent photoabsorption studies by Kelly and Simons[11] and by Swanson and Armstrong[7] have shown that the dominant ground-state correlation effects in the neighboring atom argon are those which cause virtual excitation of a pair of $3p$ electrons into excited nd orbitals. In Cl, there is the additional possibility that there are also present single-electron excitations of the type $s \rightarrow d$. Such single-electron excitations are forbidden in Ar by Brillouin's theorem, but are allowed in a non-closed-shell atom such as Cl. Consequently, we expect that the major correlation effects in the ground state of Cl will be included if we use a multiconfiguration wave function of the form

$$|\psi_i\rangle = a\,|3s^2 3p^5;^2P\rangle + \sum_{\bar{n}} \left[\sum_{i,j} d_{ij}(\bar{n})\,|3s^2 3p^3(S_i L_i)\bar{n}d^2(S_j L_j);^2P\rangle + \sum_k c_k(\bar{n})\,|3s3p^5;S_k L_k,\bar{n}d;^2P\rangle + \sum_m d'_m(\bar{n})\,|3s^0 3p^5,\bar{n}d^2(S_m L_m);^2P\rangle \right] . \quad (1)$$

This form has been obtained by using orthogonal transformations such as those suggested by Froese Fischer[12] to change $n_1 d n_2 d$ states into pairs of d-like pseudostates $\bar{n}d$. The advantage of the use of these pseudostates is that the sums over $\bar{n}$ in (1) can be expected to be rapidly converging functions of $\bar{n}$. In fact, as in the case of Ar,[7] we find that only the $\bar{n}=3$ term need be retained in order to obtain a reasonable description of the Cl ground state.

The wave functions and coefficients appearing in (1) were obtained by first evaluating Hartree-Fock (HF) wave functions for the $3s^2 3p^5;^2P$ state using a somewhat modified version of Froese Fischer's program MCHF-75.[13] These orbitals were then frozen, and a MCHF calculation was carried out to determine the $\bar{3}d$ orbitals and their mixing coefficients. The resulting coefficients are shown in Table I. Of interest are the relatively large coefficients obtained for the one-electron excitations of the type $s \rightarrow \bar{d}$. Other trial calculations were made to determine if other configurations were of importance in describing the ground state. All other configurations tried (including a set which contained $\bar{4}d$ functions also) produced mixing

TABLE I. The chlorine ground-state configurations and their corresponding mixing weights using the Condon-Shortley phase convention.

Label	Configuration	Mixing weights
1	$3s^2 3p^5;^2P$	0.975 016
2	$3s^2 3p^3\,^2P, \bar{3}d^2\,^1S;^2P$	0.098 174
3	$3s^2 3p^3\,^2P, \bar{3}d^2\,^3P;^2P$	−0.056 180
4	$3s^2 3p^3\,^2P, \bar{3}d^2\,^1D;^2P$	−0.050 942
5	$3s^2 3p^3\,^2D, \bar{3}d^2\,^3P;^2P$	−0.072 382
6	$3s^2 3p^3\,^2D, \bar{3}d^2\,^1D;^2P$	0.098 646
7	$3s^2 3p^3\,^2D, \bar{3}d^2\,^3F;^2P$	0.012 048
8	$3s^2 3p^3\,^4S, \bar{3}d^2\,^3P;^2P$	−0.064 877
9	$3s3p^5;^1P, \bar{3}d;^2P$	0.104 425
10	$3s3p^5;^3P, \bar{3}d;^2P$	−0.043 726
11	$3s^0 3p^5\,^2P, \bar{3}d^2\,^1S;^2P$	−0.040 917
12	$3s^0 3p^5\,^2P, \bar{3}d^2\,^3P;^2P$	−0.008 412
13	$3s^0 3p^5\,^2P, \bar{3}d^2\,^1D;^2P$	−0.008 264

TABLE II. The $Cl^+ 3p^4;^3P$ ionic-core configurations and their corresponding mixing weights using the Condon-Shortley phase convention.

Label	Configuration	Mixing weights
1	$3s^2 3p^4;3P$	0.976 003
2	$3s^2 3p^2\,^3P, \bar{3}d^2\,^1D;^3P$	−0.084 314
3	$3s^2 3p^2\,^3P, \bar{3}d^2\,^3P;^3P$	0.068 880
4	$3s^2 3p^2\,^3P, \bar{3}d^2\,^1S;^3P$	−0.073 718
5	$3s^2 3p^2\,^1D, \bar{3}d^2\,^3F;^3P$	−0.011 180
6	$3s^2 3p^2\,^1D, \bar{3}d^2\,^3P;^3P$	−0.061 834
7	$3s^2 3p^2\,^1S, \bar{3}d^2\,^3P;^3P$	−0.026 806
8	$3s\,3p^4\,^3P;^2P, \bar{3}d;^3P$	0.077 898
9	$3s\,3p^4\,^3P;^4P, \bar{3}d;^3P$	−0.041 577
10	$3s\,3p^4\,^1D;^2D, \bar{3}d;^3P$	−0.123 838
11	$3s^0 3p^4\,^3P, \bar{3}d^2\,^1D;^3P$	0.006 826
12	$3s^0 3p^4\,^3P, \bar{3}d^2\,^3P;^3P$	−0.007 049
13	$3s^0 3p^4\,^3P, \bar{3}d^2\,^1S;^3P$	−0.046 445
14	$3s^0 3p^4\,^1D, \bar{3}d^2\,^3F;^3P$	0.007 507
15	$3s^0 3p^4\,^1D, \bar{3}d^2\,^3P;^3P$	0.004 352
16	$3s^0 3p^4\,^1S, \bar{3}d^2\,^3P;^3P$	−0.001 390

TABLE III. The $Cl^+ 3p^4;^1D$ ionic-core configurations and their corresponding mixing weights using the Condon-Shortley phase convention.

Label	Configuration	Mixing weights
1	$3s^2 3p^4;^1D$	0.974 320
2	$3s^2 3p^2\,^3P, \bar{3}d^2\,^3F;^1D$	0.013 843
3	$3s^2 3p^2\,^3P, \bar{3}d^2\,^3P;^2D$	−0.083 155
4	$3s^2 3p^2\,^1D, \bar{3}d^2\,^1G;^1D$	−0.002 055
5	$3s^2 3p^2\,^1D, \bar{3}d^2\,^1D;^1D$	0.100 073
6	$3s^2 3p^2\,^1D, \bar{3}d^2\,^1S;^1D$	−0.073 730
7	$3s^2 3p^2\,^1S, \bar{3}d^2\,^1D;^1D$	−0.031 245
8	$3s\,3p^4\,^1S;^2S, \bar{3}d;^1D$	−0.007 666
9	$3s\,3p^4\,^3P;^2P, \bar{3}d,^1D$	0.155 682
10	$3s\,3p^4\,^1D;^2D, \bar{3}d;^1D$	−0.015 945
11	$3s^0 3p^4\,^3P, \bar{3}d^2\,^3F;^1D$	0.006 729
12	$3s^0 3p^4\,^3P, \bar{3}d^2\,^3P;^1D$	0.006 814
13	$3s^0 3p^4\,^1D, \bar{3}d^2\,^1G;^1D$	0.012 664
14	$3s^0 3p^4\,^1D, \bar{3}d^2\,^1D;^1D$	−0.012 391
15	$3s^0 3p^4\,^1D, \bar{3}d^2\,^1S;^1D$	−0.046 892
16	$3s^0 3p^4\,^1S, \bar{3}d^2\,^1D;^1D$	−0.003 127

weights which were at least one order of magnitude smaller than those of the $\bar{3}d$ configurations.

B. Final-state correlations

In Ar, final-state correlations were found to play a relatively minor role. The major correlation effects in the final state were produced by correlation in the $p^5\,^2P$ ionic parent state, and these effects could be evaluated in a straightforward way through use of the MCHF. In Cl, the problem is much more complicated. Ionization from the $3p$ subshell is likely to produce any of three low-lying states of the parent ion: $3s^2 3p^4\,^1S$, ^3P, or ^1D. In addition, ionization from the $3s$ subshell can leave the ion in either the $3s 3p^5\,^1P$ or ^3P state. Taking into account that the $3p$ can ionize into either an ϵd or an ϵs channel, and that dipole selection rules show that the final ion plus photoelectron can be in a ^2S, ^2P, or ^2D state, one finds a total of 15 possible final states:

$$
\begin{aligned}
&3p^4\,^3P,\epsilon d;^2D,\quad 3s\,3p^5;^3P,\epsilon p;^2P\ ,\\
&3p^4\,^1D,\epsilon d;^2D,\quad 3s\,3p^5;^1P,\epsilon p;^2P\ ,\\
&3p^4\,^1S,\epsilon d;^2D,\quad 3p^4\,^1D,\epsilon d;^2S\ ,\\
&3p^4\,^1D,\epsilon s;^2D,\quad 3p^4\,^1S,\epsilon s;^2S\ ,\\
&3s3p^5;^3P,\epsilon p;^2D,\quad 3s\,3p^5;^3P,\epsilon p;^2S\ ,\\
&3s\,3p^5;^1P,\epsilon p;^2D,\quad 3s\,3p^5;^1P,\epsilon p;^2S\ .\\
&3p^4\,^3P,\epsilon d;^2P\ ,\\
&3p^4\,^1D,\epsilon d;^2P\ ,\\
&3p^4\,^3P,\epsilon s;^2P\ ,
\end{aligned}
\tag{2}
$$

As in the Ar study,[7] we evaluated correlation effects within the $p^{4\,2S+1}L$ parent states of the ion by using a CI calculation based on the wave functions obtained in the ground-state MCHF. In order to keep the types of correlation included in the final state similar to that included in the initial state, we obtained the final-state wave function

TABLE IV. The $Cl^+ 3p^4;^1S$ ionic-core configurations and their corresponding mixing weights using the Condon-Shortley phase convention.

Label	Configuration	Mixing weights
1	$3s^2 3p^4;^1S$	0.960 571
2	$3s^2 3p^2\,^3P, \bar{3}d^2\,^3P;^1S$	−0.083 280
3	$3s^2 3p^2\,^1D, \bar{3}d^2\,^1D;^1S$	−0.101 354
4	$3s^2 3p^2\,^1S, \bar{3}d^2\,^1S;^1S$	0.149 805
5	$3s\,3p^4\,^1D;^2D, \bar{3}d;^1S$	−0.062 243
6	$3s^0 3p^4\,^3P, \bar{3}d^2\,^3P;^1S$	0.017 176
7	$3s^0 3p^4\,^1D, \bar{3}d^2\,^1D;^1S$	0.017 448
8	$3s^0 3p^4\,^1S, \bar{3}d^2\,^1S;^1S$	−0.015 460
9	$3s^0 3p^6;^1S$	0.181 497

by diagonalizing the Hamiltonian within the manifold of states arising from the configurations $3s^2 3p^4$, $3s^2 3p^2 \bar{3}d^2$, $3s 3p^4 \bar{3}d$, $3p^4 \bar{3}d^2$, and $3p^6$. The mixing coefficients obtained in this way are shown in Tables II–IV.

Again following the approach used successfully in the Ar calculation,[7] we evaluated continuum wave functions for all the $3s^2 3p^4$ channels by defining a $V^{N-1}(\gamma SL)$ potential using the multiconfiguration ionic states obtained above [$\mathrm{MC}V^{N-1}(\gamma SL)$]. As in the Ar work, terms in the $\mathrm{MC}V^{N-1}(\gamma SL)$ involving products of the small weights corresponding to configurations other than $3s^2 3p^4$ were dropped. Detailed expressions for the resulting $\mathrm{MC}V^{N-1}$ potentials can be found in Ref. 10.

All final states corresponding to a given value of total spin, orbital angular momentum, and parity are mixed together by the Coulomb interaction. We have evaluated this mixing using the K-matrix approach. In this method, the correct jth final-state eigenfunction corresponding to a state of total-energy E can be written as[10,14]

$$
|j,E\rangle = \sum \left(|i,E) + \sum_l \mathscr{P} \frac{\int |l,E')K(l,E';i,E)}{E-E'} dE' \right) B_i^j(E), \tag{3}
$$

where the $|i,E)$ states correspond to single-channel states obtained by coupling a continuum wave function calculated in a $\mathrm{MC}V^{N-1}(\gamma SL)$, to a CI ionic wave function to give a particular total S and L. The numbers i,j, etc., designate all the quantum numbers involved, and $\mathscr{P}$ indicates principal-value integration. The B_i^j give $|j,E\rangle$ the desired asymptotic form; that is, that it asymptotically describes a photoelectron in the jth channel. The K-matrix elements satisfy the integral equation

$$
K(j,\bar{E};i,E) = (j,\bar{E}\,|\,H'\,|\,i,E) + \sum_l \mathscr{P} \frac{\int (j,\bar{E}\,|\,H'\,|\,l,E')K(l,E';i,E)}{E-E'} dE' \tag{4}
$$

and the coefficients $B_i^k(E)$ satisfy the algebraic equations

$$
\sum_l (1 - i\pi K)_{jl} B_l^k(E) = \delta(j,k)\ , \tag{5}
$$

where H' is the residual-interaction Hamiltonian.

The principal-value integrals in (3) and (4) are, in reali-

ty, sums over bound states and integrals over continua. Inclusion of bound states in these expressions means that the effects of autoionizing resonances will automatically be included in our results.

The number of bound states included in this calculation was determined by terminating the sum over bound states when the difference in energy between two consecutive bound states was less than 0.007 a.u. This corresponded to keeping only the four lowest-energy bound states in each channel. Contributions due to higher bound states were included by continuum normalizing the higher bound states using the factor

$$\left[\frac{dn}{dE}\right]^{1/2}_{E=E_n}=(-2E_n)^{-3/4} \tag{6}$$

and beginning the continuum integration at approximately the position of the fourth lowest-energy bound state.

The upper limit of integration in each case was chosen by verifying that reasonable changes in these limits did not significantly affect the values of the integrals. The upper limits varied from channel to channel, being as low as 2.68 a.u. for the states having a $3p^4\,{}^3P$ core, and as high as 4.48 a.u. for some states having a $3p^4\,{}^1D$ or ${}^1S$ ionic core. Between 30 and 50 values of the continuum wave functions were used in each case.

Equation (4) is solved using a modified version of a program of Starace.[15] This program approximates K and the matrix element of H' by three-point quadratic functions; the integrals can then be carried out analytically, producing algebraic equations which can be solved using standard techniques.

In setting up our K-matrix equation, we used experimental energies of the 3s and 3p subshell ionization thresholds.[16,17] For the $3p^4$ states of Cl^+, we used 0.478 10 a.u. (${}^3P$), 0.529 63 a.u. (${}^1D$), and 0.603 56 a.u. (${}^1S$). For the $3s\,3p^5$ states, we used 0.903 90 a.u. (${}^3P$) and 1.0040 a.u. (${}^1P$).

Because of limitations imposed by the computer used, we were unable to couple all of the channels belonging to each multiplet. We generally were unable to couple more than three channels, although for the case of the ${}^2S$ multiplet, we were also able to include coupling to an additional single bound state, $3s\,3p^6\,{}^2S$. As a result of these limitations, we were, of course, able to obtain only approximate eigenfunctions of H.

Our decisions concerning which of the many possible channels to couple were based in large part on the results of several calculations involving the ${}^2S$ channels. These studies, which we discuss in Sec. IV, offered suggestions as to which of the couplings were the most important. One generally accepted result which was shown to also hold in the present case was that channels having small independent-channel cross sections have little effect on channels having a large independent-channel cross section when the channels are coupled. Thus, the $3p\rightarrow\epsilon s$ channels had little effect on the dominant $3p\rightarrow\epsilon d$ channels when coupling was introduced. In addition, the rather weak excitations of the type $3s\rightarrow\epsilon p$ are also generally not expected to have a significant effect on the $3p\rightarrow\epsilon d$ channels. The exception to this last statement occurs in the channels having a ${}^2S$ final state; in this case, there is an important excited bound state $3s\,3p^6\,{}^2S$ which produces a major perturbation in the corresponding $3p\rightarrow\epsilon d$ channels.

III. PROCEDURE

Using the states described in Sec. II, we evaluate the partial photoabsorption cross section to the jth channel as a function of photon energy ω, which is related to the energy E of the final state $|j,E)$ and the energy E_0 of the initial state ψ_i by

$$\omega+E_0=E$$

using

$$\sigma_j(\omega)=\tfrac{2}{9}\pi^2\alpha a_0^2\omega\,|\,(j,E||T^{(01)}||\psi_i\rangle\,|^2\ . \tag{7}$$

The total photoionization cross section at ω is then obtained by summing over all channels which are accessible at the photon energy ω. The operator $T^{(01)}$ is the dipole transition operator, which is given by

$$T^{(01)}=T_L^{(01)}=\sum_{j=1}^{N}\vec{r}_j \tag{8}$$

in the length gauge, and by

$$T^{(01)}=T_V^{(01)}=\sum_{j=1}^{N}\frac{\vec{p}_j}{i\omega} \tag{9}$$

in the velocity gauge. The reduced matrix element in (7) is evaluated in atomic units.

We have also studied the photoelectron angular distribution using the states described in Sec. II. In the case that linearly polarized light is used, the distribution can be described by the general formula

$$\frac{d\sigma(j,\omega)}{d\Omega}=\frac{\sigma(j,\omega)}{4\pi}[1+\beta(\omega)P_2(\hat{e}\cdot\hat{k})]\ , \tag{10}$$

where $\sigma(j,\omega)$ is the total photoionization cross section at ω corresponding to the ion being left in state $j=(\gamma_jS_jL_j)$, P_2 is the second-order Legendre polynomial whose argument is the cosine of the angle between the polarization vector $\hat{e}$ of the incident radiation and the direction $\hat{k}$ of the photoelectron momentum, and $d\Omega$ is the solid angle into which the photoelectron is scattered. With appropriate redefinition of β and the vector $\hat{e}$ Eq. (10) also gives the cross section in an unpolarized field, the case we studied. The asymmetry parameter $\beta(\omega)$ $(-1\le\beta\le 2)$ contains all of the information concerning the geometric and dynamic properties of the initial $|\gamma_0S_0L_0\rangle$ and final $|\gamma_jS_jL_j,\epsilon l_j;SL\rangle$ states[10,18]

$$\begin{aligned}\beta(\omega)=(-1)^{L_0+L_j}&\frac{20\pi^2\alpha a_0^2\omega[S_0,L_0]^{-1}}{\sigma_{j(i)}(\omega)}\begin{bmatrix}1&1&2\\0&0&0\end{bmatrix}\\
&\times\sum_{\substack{l_j,l_j',\\L,L'}}i^{(l_j-l_j')}e^{-i(P_j-P_j')}[l_j,l_j',L,L']^{1/2}\begin{bmatrix}l_j'&l_j&2\\0&0&0\end{bmatrix}\begin{Bmatrix}L&2&L'\\l_j'&L_j&l_j\end{Bmatrix}\begin{Bmatrix}1&1&2\\L'&L&L_0\end{Bmatrix}\\
&\times\langle\gamma_jS_jL_j,l_j;SL||T^{(01)}||\gamma_0S_0L_0\rangle\langle\gamma_jS_jL_j,l_j';SL'||T^{(01)}||\gamma_0S_0L_0\rangle^*\delta_{S,S_0}\ .\end{aligned} \tag{11}$$

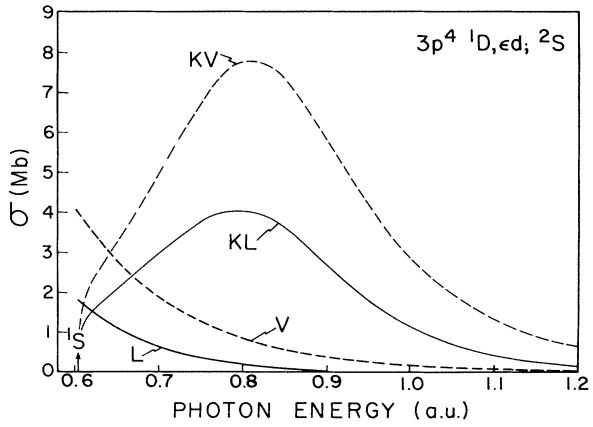

FIG. 1. Photoabsorption cross sections for the $3p^4\,^1D,\epsilon d;^2S$ channel using both the single- and coupled-channel ($3p^4\,^1D,\epsilon d;^2S$, $3p^4\,^1S,\epsilon s;^2S$, and $3s\,3p^6;^2S$) final states. *L*, single-channel length; *V*, single-channel velocity; *KL*, *K*-matrix length; *KV*, *K*-matrix velocity.

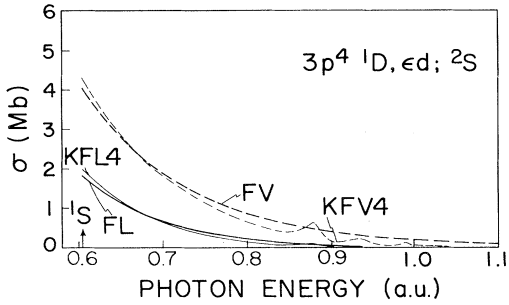

FIG. 2. Photoabsorption cross sections for the $3p^4\,^1D,\epsilon d;^2S$ channel using both the single- and coupled-channel ($3p^4\,^1D,\epsilon d;^2S$, $3s\,3p^5;^3P,\epsilon p;^2S$, $3s\,3p^5;^1P,\epsilon p;^2S$, and $3s\,3p^6;^2S$) final states. *FL*, single-channel length; *FV*, single-channel velocity; *KFL* 4, *K*-matrix length; *KFV* 4, *K*-matrix velocity.

When the wave functions of Sec. II are used, P_j is given by the Coulomb phase shift. If one wishes to make comparisons with β calculated without channel coupling (without using the *K* matrix), one can use (11) by replacing the states $|\gamma S_j L_j,\epsilon l_j;SL\rangle$ by their single-channel equivalents, and letting P_j be equal to the Coulomb phase shift plus the non-Coulombic phase shift induced in the *j*th channel by $\mathrm{MC}V^{N-1}(\gamma SL)$.

IV. PARTIAL CROSS SECTIONS

A. The ^2S channels

In the ^2S case, there are only four channels to be considered, and a reasonably thorough study was possible. Our preliminary calculations, the results of Brown *et al.*,[5] and the results of Cowan *et al.*,[19] showed that there is a very strong interaction between the $3s3p^6;^2S$ and $3p^4\,^1D,\epsilon d;^2S$ channels. Consequently, this bound state was included in all of the studies we made of the ^2S channels.

In the independent-channel model, the $3s\,3p^6;^2S$ lies above the ^1D ionization limit; experimentally, however, it is found to lie at 0.390 378 a.u., which is below the energy of the $3p^4\,^1D,3d;^2S$ state. It was not possible in our calculation to say directly whether the configuration interaction introduced through use of the *K* matrix resulted in the $3s3p^6;^2S$ level being shifted to its experimentally observed position. In order to check the consistency of our wave functions and procedure, however, we did calculate the position of the $3s3p^6;^2S$ state, assuming that it is interacted only with the $3p^4\,^1D,\epsilon d;^2S$ channel. Cowan *et al.*[19] have determined that this is, indeed, the dominant interaction. In this case, the isolated resonance approach of Fano[20] can be employed. Using the ground-state orbitals, probably a poor approximation, we determined the energy of the $3s3p^6;^2S$ state, in the absence of channel interaction, to be 0.566 119 a.u. We then coupled this state to the $3p^4\,^1D,\epsilon d;^2S$ channel, producing an energy shift to 0.418 619 a.u., relatively close to the experimental value.

Results obtained by coupling the three channels $3p^4\,^1D,\epsilon d;^2S$, $3p^4\,^1S,\epsilon s;^2S$, and $3s\,3p^6;^2S$ are shown in Fig. 1, with results being shown for both coupled-channel (*KL* and *KV*) and uncoupled-channel (*L* and *V*) results. (In this case, as in all other cases discussed below, calculations were carried out for a wide variety of approximations for the final and initial states. Details of these other calculations and the results obtained can be found in Ref. 10. The large maxima at about 0.8-a.u. photon energy is due to the $3s\,3p^6;^2S$ state. A similar calculation done without the $3p^4\,^1S,\epsilon s;^2S$ channel showed only minor changes, with the main effect being near the ^1S edge.

The result shown in Fig. 1 can be compared with that obtained in a similar calculation of Brown *et al.*,[5] who obtained a qualitatively similar result. The maximum of their partial cross section is somewhat lower than ours, however. This difference may possibly be attributable to their using the experimental $3s\,3p^6;^2S$ energy in their calculation, while we used our calculated value of 0.566 119 a.u.

The inclusion of the higher terms in the $3s\,3p^5np$ series greatly altered the results observed when only the $3s\,3p^6$ was kept. Figure 2 shows the photoionization cross section obtained when the $3p^4\,^1D,\epsilon d;^2S$, $3s\,3p^5\,^1P,\epsilon p;^2S$, $3s\,3p^5\,^3P,\epsilon p;^2S$, and $3s\,3p^6;^2S$ channels are coupled. It is obvious that the effect produced by the $3s\,3p^{5\,2S+1}P,\epsilon p;^2S$ states nearly cancels that of the $3s\,3p^6;^2S$ state. Further studies showed that it was the $3s\,3p^5\,^3P,\epsilon p;^2S$ channel which produced almost all of this cancellation. Our conclusion, therefore, was that the $3s\,3p^5\epsilon p$ series, including the $3s\,3p^6$ state, has almost no discernable effect on the $3p^4\,^1D,\epsilon d;^2S$ partial cross sections.

Although the weaker channels do not significantly affect the stronger channels when channel coupling is considered, the converse is certainly not true. In the ^2S case, we were also able to do a fairly thorough study of the effects of channel coupling on the weaker channels. Using the same four-channel coupling scheme as discussed in the previous paragraph, we examined the cross sections for the channels resulting from a $3s\rightarrow\epsilon p$ transition; namely, the $3s\,3p^5;^3P,\epsilon p;^2S$ and $3s\,3p^5;^1P,\epsilon p;^2S$ channels, in order to evaluate channel-interaction effects in the proximity of

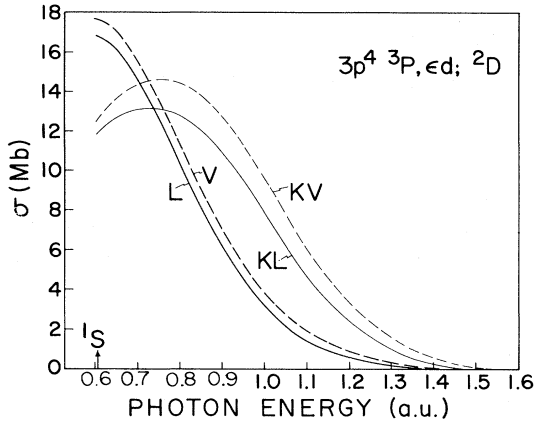

FIG. 3. Photoabsorption cross sections for the $3p^4\,{}^3P,\epsilon d;{}^2D$ channel. *L*, single-channel length; *V*, single-channel velocity; *KL*, *K*-matrix length; *KV* *K*-matrix velocity.

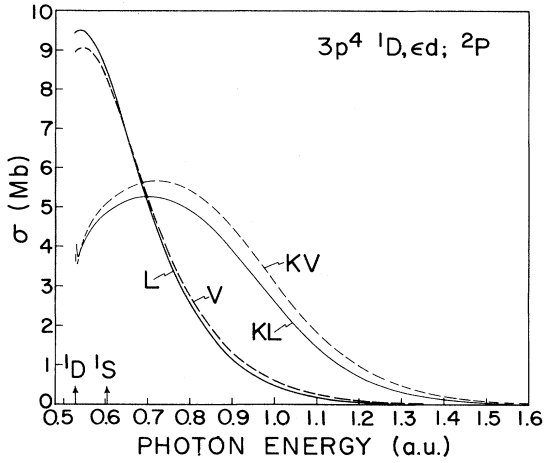

FIG. 4. Photoabsorption cross sections for the $3p^4\,{}^1D,\epsilon d;{}^2P$ channel. *L*, single-channel length; *V*, single-channel velocity; *KL*, *K*-matrix length; *KV*, *K*-matrix velocity.

their respective thresholds. In both channels the Hartree-Fock cross sections (length) are small at the ionic thresholds, being 0.002 and 0.004 Mb, respectively, for the $3s3p^5;{}^3P,\epsilon p;{}^2S$ and $3s3p^5;{}^1P,\epsilon p;{}^2S$ channels. At 0.008 Mb, the reaction matrix cross section is also small at threshold for the $3s3p^5;{}^3P,\epsilon p;{}^2S$ channel; however, it is an order of magnitude larger than the HF value for the $3s3p^5;{}^1P,\epsilon p;{}^2S$ channel, which is 0.06 Mb. Just above the ionic threshold of each channel, the channel-interaction curves increase rapidly, whereas the single-channel result decreases to at least an order of magnitude below that of the *K*-matrix values.

As a final investigation of the partial cross sections for the ^2S multiplet, we studied the effect of interchannel coupling on the $3p^4\,{}^1S,\epsilon s;{}^2S$ channel, which has small photoabsorption cross sections in the independent-channel approximation relative to those for the $3p^4\,{}^1D,\epsilon d;{}^2S$ channel. In this evaluation of the transition probabilities, we coupled the $3p^4\,{}^1D,\epsilon d;{}^2S$, $3p^4\,{}^1S,\epsilon s;{}^2S$, and $3s3p^6;{}^2S$ channels, along with either the $3s3p^5;{}^3P,\epsilon p;{}^2S$ or the $3s3p^5;{}^1P,\epsilon p;{}^2S$ channel. As in the case of the $3p^4\,{}^1D,\epsilon d;{}^2S$ calculation described above, we found that when the $3s3p^5;{}^3P,\epsilon p;{}^2S$ channel was included, the resulting $3p^4\,{}^1S,\epsilon s;{}^2S$ cross sections were nearly identical to the independent-channel results. That is, once again the $3s3p^5;{}^3P,\epsilon p;{}^2S$ channel balanced out the interaction effect of the $3s3p^6;{}^2S$ discrete state. Somewhat unexpectedly in this case, it also canceled out most of the effect produced by the $3p^4\,{}^1D,\epsilon d;{}^2S$ channel on the transition probabilities to the $3p^4\,{}^1S,\epsilon s;{}^2S$ channel. Again as in the previous $3p^4\,{}^1D,\epsilon d;{}^2S$ calculation, the $3s3p^5;{}^1P,\epsilon p;{}^2S$ channel had negligible influence on the coupled-channel cross sections. We note that there are no published channel-interaction cross-section values with which to compare our four-channel evaluations for either the $3p^4\,{}^1D,\epsilon d;{}^2S$ or $3p^4\,{}^1S,\epsilon s;{}^2S$ channels.

B. The ^2P and ^2D channels

Based on the results obtained in the ^2S channel, it seemed reasonable to assume that the dominant interactions in the ^2D and ^2P channels are those between the channels of the type $3p^4\epsilon d$ corresponding to different *LS* states of the $3p^4$ ionic core. Consequently, the only channel-interaction effects in our calculations for the ^2D final state come from coupling the $3p^4\,{}^3P,\epsilon d;{}^2D$, $3p^4\,{}^1D,\epsilon d;{}^2D$, and $3p^4\,{}^1S,\epsilon d;{}^2D$ channels. For the ^2P final state, the coupling considered was between the $3p^4\,{}^3P,\epsilon d;{}^2P$ and $3p^4\,{}^1D,\epsilon d;{}^2P$ channels.

Typical results obtained from these calculations are shown in Fig. 3 ($3p^4\,{}^3P,\epsilon d;{}^2D$) and Fig. 4 ($3p^4\,{}^1D,\epsilon d;{}^2P$), where one sees partial cross sections calculated both without (*L*,*V*) and with (*KL*,*KV*) interchannel coupling. In all cases, the MCHF initial and final states are used.

One sees that the coupled-channel results are depressed relative to the single-channel results at the highest threshold for each channel. As a consequence, the coupled-channel results all show delayed maxima, while the single-channel results are very near their maxima at threshold.

These coupled-channel cross sections can be compared with the results of Brown *et al.*,[5] even though we have included some kinds of electron correlation in the ionic state which they have not. In the photon-energy region near the ionization threshold for the Cl^+ $3p^4;{}^1S$ state, where relaxation effects would be expected to be most important, the geometric mean of our curves shows excellent agreement with the relaxed core curves of Brown *et al.*, differing by no more than a few percent (Brown *et al.* report only the geometric mean of their length and velocity result in this case). At high photon energies (at least as great as 0.90 a.u.), where we anticipate the unrelaxed core results of Brown *et al.* to be more indicative of the physical process than their relaxed core results, the geometric mean of our coupled-channel cross sections lies within 5—10% but slightly below the unrelaxed curve of Brown *et al.* Although we utilize an unrelaxed ionic orbital basis set throughout the MCHF calculation, incorporating electron correlation in the residual ion through a multiconfiguration description of the ionic core allows for a certain

TABLE V. The percentage difference between the length and velocity channel-interaction cross sections for the ^2D and ^2P channels at the photon energy 0.6108 a.u. (near the $3p^4;^1S$ ionic threshold).

Channel	Brown[a] Relaxed	Brown[a] Unrelaxed	Present Results
$3p^4\,^3P,\epsilon d;^2D$	8	9	6
$3p^4\,^1D,\epsilon d;^2D$	11	6	17
$3p^4\,^1S,\epsilon d;^2D$	26	26	14
$3p^4\,^3P,\epsilon d;^2P$	22	14	4
$3p^4\,^1D,\epsilon d;^2P$	23	22	5

[a]Channel-interaction calculation of Brown *et al.*, Ref. 5.

amount of the ionic relaxation effects to be included. This results in the good agreement between the MCHF geometric mean and the relaxed basis curve of Brown *et al.*[5] for photon energies in the vicinity of the ^1S ionic threshold.

The most interesting feature of our partial cross-section spectra in the ^2P final state occurs in the $3p^4\,^1D,\epsilon d;^2P$ channel; that being the sharp dip in the length and velocity K-matrix profiles (KL and KV, respectively) just above the $Cl^+\ 3p^4;^1D$ threshold (0.529 63 a.u.) (Fig. 4). The origin of this feature is not clear. Subsequent to its discovery we conducted several additional calculations, attempting to determine if the anomaly was a product of the K-matrix procedure. Employing fewer bound orbitals with both the same and different energy meshes in the vicinity of the dip produced cross-section curves qualitatively similar to the initial ones but with varying degrees of depth and breadth. Although it is possible that an energy mesh with a much greater density of points in the vicinity of the ^1D threshold might eliminate this feature (such a calculation was not feasible for us), our investigations lead us to believe that the behavior is real. Unfortunately, Brown *et al.*[5] do not present any cross sections below the ^1S threshold, and we are therefore unable to compare results in the region between the ^1D and ^1S thresholds where the dip occurs.

How our photoabsorption cross sections for the ^2D and ^2P final states compare with those of Brown *et al.*[5] can be seen in Table V, which shows the relative differences between the length and velocity channel-interaction cross sections for the two methods at the photon energy 0.6108 a.u., just above the ^1S ionization threshold (0.603 56 a.u.). It is clear that in this low-energy portion of the spectrum, where a relaxed-basis calculation is expected to be more accurate than one employing an unrelaxed basis, the relative length-velocity separation of Brown *et al.* is larger than our length-velocity difference except in the $3p^4\,^1D,\epsilon d;^2D$ channel.

Unfortunately, because of the large number of channels involved in the ^2D and ^2P cases, we were unable to investigate the effects of the "large" $3p\rightarrow\epsilon d$ transitions on the "small" $3p\rightarrow\epsilon s$ and $3s\rightarrow\epsilon p$ cross sections.

C. Comparison of partial cross sections with results of other investigations

The only experimental partial photoionization cross-section measurements extant for chlorine are some indirect observations by Kimura *et al.*[21] These data consist of ratios of the partial cross sections for the channels possessing the three ionic-core multiplets $Cl^+\ 3p^4$ at a single photon energy: 21.2 eV (0.7791 a.u.). Table VI presents the ratios of the single- and coupled-channel cross sections relative to the values for the ionic core $Cl^+\ 3p^4;^3P$, multiplied by the factor 1.5, in the length and velocity formulations. Also exhibited are the ratios found in the reaction-matrix MBPT and Hartree-Fock calculations of Brown *et al.*[5] using both their relaxed and unrelaxed basis sets, the length ratios from the independent-channel RPAE results of Starace and Armstrong,[2] and the experimental ratios. The MCHF K-matrix ratios in Table VI include contributions from the cross sections to all permitted channels arising from a $3p\rightarrow\epsilon d$ dipole transition and the $3p\rightarrow\epsilon s$ cross sections obtained from the coupled-channel calculation of the $3p^4\,^1S,\epsilon s;^2S$ channel. The remaining theoretical ratios in Table VI contain contributions from all allowed $3p\rightarrow\epsilon s$ transitions calculated in the single-channel approximation. In obtaining our channel-interaction ratios, we used the cross sections for the $3p^4\,^1D,\epsilon d;^2S$ channel which were determined by coupling the $3p^4\,^1D,\epsilon d;^2S$, $3s\,3p^5;^3P,\epsilon p;^2S$, $3s\,3p^5;^1P,\epsilon p;^2S$, and $3s\,3p^6;^2S$ channels. Analogously, the coupled-channel cross sections employed for the $3p^4\,^1S,\epsilon s;^2S$ channel were those found by coupling the $3p^4\,^1D,\epsilon d;^2S$, $3p^4\,^1S,\epsilon s;^2S$, $3s\,3p^5;^3P,\epsilon p;^2S$, and $3s\,3p^6;^2S$ channels.

Comparison of the various numbers given in Table VI

TABLE VI. Ratios of the chlorine photoabsorption length (velocity) partial cross sections relative to those for the ionic multiplet $Cl^+\ 3p^4;^3P$ (multiplied by 1.5) at the photon energy 0.7791 a.u.

Method	^3P	^1D	^1S
Brown *et al.*[a] (relaxed)	1.500(1.500)	0.743(0.790)	0.128(0.144)
Brown *et al.*[a] (unrelaxed)	1.500(1.500)	0.685(0.718)	0.106(0.124)
Hartree-Fock[a] (relaxed)	1.500(1.500)	0.702(0.834)	0.176(0.195)
Hartree-Fock[a] (unrelaxed)	1.500(1.500)	0.453(0.585)	0.109(0.132)
Starace and Armstrong[b]	1.500	0.57	0.18
MCHF[c]	1.500(1.500)	0.779(0.828)	0.194(0.185)
Experiment[d]	1.5	0.81	0.16

[a]Channel-interaction calculation of Brown *et al.*, Ref. 5.
[b]Open-shell RPAE calculation of Starace and Armstrong, Ref. 2.
[c]Uses the four-channel K-matrix cross sections for the $3p^4\,^1D,\epsilon d;^2S$ and $3p^4\,^1S,\epsilon s;^2S$ channels.
[d]Experiment of Kimura *et al.*, Ref. 21.

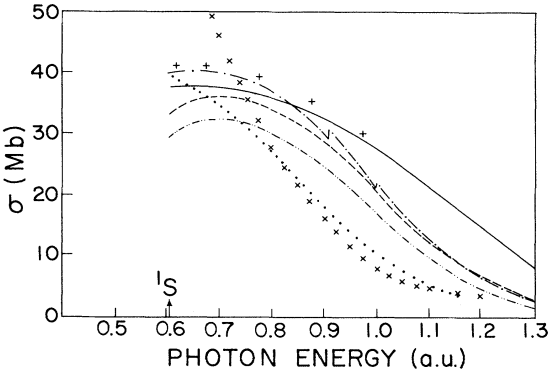

FIG. 5. Comparison of the channel-interaction total photoabsorption cross sections for $3p \rightarrow \epsilon d$ transitions with other theoretical calculations. + + + +, close-coupling calculation of Conneely (Ref. 1); —, R-matrix calculation of Lamoureux and Combet Farnoux (Ref. 4); —·—·, MBPT calculation of Brown *et al.* (Ref. 5); . . ., open-shell RPAE (Ref. 3); ××××, open-shell RPAE (independent-channel) calculation (Ref. 2); — — —, MCHF K-matrix velocity; —··—··, MCHF K-matrix length.

shows that no theoretical calculation exactly reproduces the experimental results. The present results and the relaxed results of Brown *et al.* are both, however, in reasonable agreement with experiment.

V. TOTAL CROSS SECTIONS

In order to determine the total photoabsorption cross sections of chlorine, we have summed the channel-interaction partial photoionization cross sections as a function of photon energy for the six ϵd channels. There has been no inclusion of either the ϵs- or ϵp-channel contributions to the total cross sections since, with the exception of the ^2S final state, we were unable to incorporate the effects of interchannel coupling on those particular transition probabilities.

Figure 5 illustrates the MCHF K-matrix total cross-section curves as well as the results of several other investigations for photon energies above the ^1S ionization threshold. Several comments concerning these total photoabsorption cross-section spectra should be made. (i) The cross sections of Brown *et al.*[5] are those obtained with their unrelaxed orbital basis set. (ii) With the exception of the present result, all profiles show only the length form of the transition probabilities. (iii) All cross-section curves, other than the open-shell independent-channel RPAE evaluation of Starace and Armstrong,[2] utilize some kind of interchannel-coupling procedure. (iv) Except for the MBPT calculation of Brown *et al.*,[5] all total cross-section profiles account only for ionization from the $3p$ subshell. The spectrum of Brown *et al.* also includes partial cross sections to channels reached by $3s \rightarrow \epsilon p$ dipole transitions; however, the Wigner cusps at the thresholds for the two states $Cl^+ 3s3p^5;^3P$ (0.903 90 a.u.) and $Cl^+ 3s3p^5;^1P$ (1.0040 a.u.) imply that only independent-channel values were used for channels having a $3s3p^5$ ionic configuration. In addition, they also employed independent-channel partial cross sections for channels produced by $3p \rightarrow \epsilon s$ transitions in determining the total cross sections.

In the vicinity of the ^1S edge, both the length and velocity MCHF K-matrix cross sections are lower than those of the other channel-interaction theories, due in part, at least, to our neglect of the transition probabilities to the ϵs channels. Starting at a photon energy of about 0.95 a.u., our correlated final-state velocity curve differs from the profile of Brown *et al.*[5] by no more than about 3% (less than about 8% for the length curve). If we allow for the single-channel partial cross sections for the ^2S channels resulting from a $3s \rightarrow \epsilon p$ transition, as do Brown *et al.*, the MCHF reaction-matrix total cross sections would be even closer in agreement with the values of Brown *et al.*

In the neighborhood of the ^1S edge, the close-coupling calculation of Conneely[1] can barely be distinguished from the MBPT curve of Brown *et al.*[5] By a photon energy of about 0.85 a.u., the MBPT values fall below the R-matrix curve[4] which declines more slowly at high photon energies (above 0.95 a.u.) than do all the other channel-interaction profiles. The independent-channel open-shell RPAE calculation[2] shows similar behavior to our uncoupled HF spectra (not shown): that being a very large amplitude at the ^1S edge, which decreases rapidly with increasing photon energy until 1.1 a.u., at which point it joins most of the coupled-channel curves. The RPAE evaluation of Cherepkov and Chernysheva[3] agrees with the other total cross sections only in the vicinity of the ^1S ionic threshold, displaying considerable divergence from these curves for photon energies larger than 0.75 a.u.

Most of the total cross-section spectra agree reasonably well for photon energies greater than 1.1 a.u., regardless of whether they were obtained with an independent- or coupled-channel method. The implication is that the effect of interchannel coupling is less significant in this region of photon energy than for lower energies. On the other hand, the R-matrix profile[4] reveals unusually large cross sections at high photon energies (at least twice as large as other theories at 1.3 a.u.), which would lead one to the opposite conclusion: that interchannel coupling is still strong even in this region of high photon energies. Nevertheless, the preponderance of theoretical studies tends to suggest that the R-matrix calculation predicts cross sections which are too large at high photon energies.

Comparing the coupled-channel total cross sections of this work with the single-channel RPAE result of Starace and Armstrong[2] and with our own single-channel HF results (not shown) enables us to comment on the characteristic differences between the channel-interaction and single-channel cross sections. It is evident from Fig. 5 that the use of some form of channel-interaction procedure in determining transition probabilities leads to depressed cross sections values in the neighborhood of the $Cl^+ 3p^4;^1S$ threshold relative to those obtained in an independent-channel calculation. As the photon energy increases, most channel-interaction profiles (the exception being the RPAE curve of Cherepkov and Chernysheva[3]) have a delayed maximum (or are relatively flat) above the ^1S edge, followed by a more gradual decline of their cross-section values than that experienced by the independent-channel result which decreases very rapidly. In other words, interchannel coupling serves to enhance transition probabilities over their single-channel values for

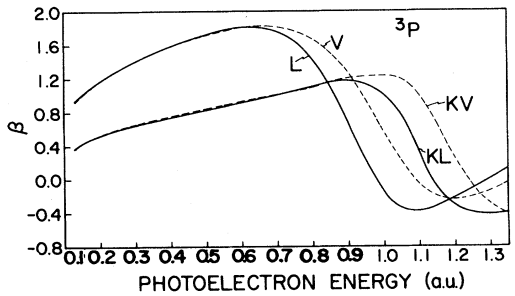

FIG. 6. Asymmetry parameters for the ionic multiplet $Cl^+ 3p^4;^3P$ (including the $3p^4\,^3P,\epsilon d;^2D$, $3p^4\,^3P,\epsilon d;^2P$, and $3p^4\,^3P,\epsilon s;^2P$ channels) using both the single- and coupled-channel final states. *L*, single-channel length; *V*, single-channel velocity; *KL*, *K*-matrix length; *KV*, *K*-matrix velocity.

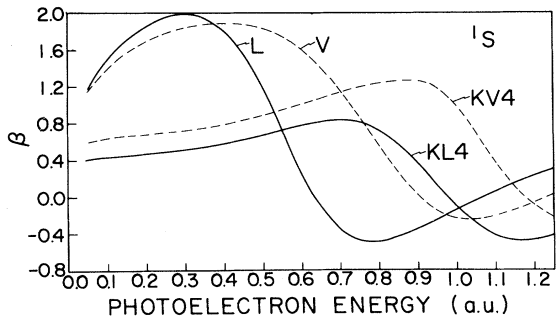

FIG. 8. Asymmetry parameters for the ionic multiplet $Cl^+ 3p^4;^1S$ (including the $3p^4\,^1S,\epsilon d;^2D$ and $3p^4\,^1S,\epsilon s;^2S$ channels). *L*, single-channel length; *V*, single-channel velocity; *KL*4, *K*-matrix length (four-channel *K* matrix for the $3p^4\,^1S,\epsilon s;^2S$ channel); *KV*4, *K*-matrix velocity (four-channel *K* matrix for the $3p^4\,^1S,\epsilon s;^2S$ channel).

photon energies somewhat above the ^1S ionic threshold. At large photon energies channel interaction is less important with the independent- and coupled-channel curves approaching one another.

VI. DIFFERENTIAL CROSS SECTIONS (ASYMMETRY PARAMETERS)

The MCHF evaluations of asymmetry parameters for the ionic multiplets arising from the 3*p*-subshell ionization of neutral chlorine, in both the independent-channel and channel-interaction (*K*-matrix) methods are shown in Figs. 6—8. For each of the three $Cl^+ 3p^4$ multiplets, the values of β have been determined using both the length and velocity forms of the correlated final-state dipole matrix elements.

In calculating the asymmetry parameters, we recognized the necessity of including the ϵs channels which were not included in the partial cross-section study. These channels are important since the $3p \rightarrow \epsilon s$ transition can greatly affect the β parameters in the neighborhood of the Cooper minimum of a $3p \rightarrow \epsilon d$ transition. An additional complicating factor in the present case is that except for the ^1S term, each ionic multiplet belongs to more than one channel arising through a $3p \rightarrow \epsilon d$ transition. Consequently, there is more than one Cooper minimum (in the single-channel approximation) for $3p \rightarrow \epsilon d$ transitions, each occurring at slightly different energies. The dipole matrix elements for the $3p \rightarrow \epsilon s$ transition channel are still important in this extended region of Cooper minima, but in a much less significant fashion than in cases where there is only one ϵd channel, such as the rare gases.

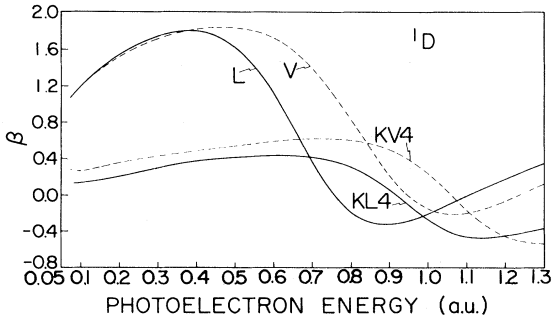

FIG. 7. Asymmetry parameters for the ionic multiplet $Cl^+ 3p^4;^1D$ (including the $3p^4\,^1D,\epsilon d;^2D$, $3p^4\,^1D,\epsilon d;^2P$, $3p^4\,^1D,\epsilon d;^2S$, and $3p^4\,^1D,\epsilon s;^2D$ channels). *L*, single-channel length; *V*, single-channel velocity; *KL*4, *K* matrix length (four-channel *K* matrix for the $3p^4\,^1D,\epsilon d;^2S$ channel); *KV*4, *K*-matrix velocity (four-channel *K* matrix for the $3p^4\,^1D,\epsilon d;^2S$ channel).

Since, as explained above, we were unable to evaluate coupled-channel $3p \rightarrow \epsilon s$ cross sections in the general case, one must ask if the use of the independent-channel transition matrix elements for the ϵs channels in the determination of the channel-interaction β coefficients might lead to considerable error. We believe that it does not. It is true that the ϵd channels will affect the transition amplitudes and cross sections for the ϵs channels in the vicinity of threshold. However, in this region of photon energy, the asymmetry parameters are relatively insensitive to the contributions of the ϵs channels, owing to the dominant transition probabilities for the ϵd channels. In the region of the "Cooper minima," preliminary calculations indicate that the channel-interaction values of the dipole amplitudes for the ϵs channels are quite similar to those obtained in the absence of channel coupling. This is due, of course, to the small size of the ϵd-channel cross sections in this photon-energy region. Thus, while it is not completely valid, one is probably justified in employing the single-channel evaluation of the transition amplitudes for the ϵs channels in the calculation of the β coefficients.

The length and velocity forms of the independent-channel and coupled-channel asymmetry parameters for the ^3P ionic term are illustrated in Fig. 6. This calculation includes contributions from the three channels: $3p^4\,^3P,\epsilon d;^2D$, $3p^4\,^3P,\epsilon d;^2P$, and $3p^4\,^3P,\epsilon s;^2P$. Hartree-Fock values of the dipole matrix elements were used for the $3p^4\,^3P,\epsilon s;^2P$ channel in computing the channel-interaction parameters, while the couplings described in Secs. IV and V were employed in obtaining the cross sections for the other channels.

Figure 7 shows the independent-channel and channel-

interaction parameters for the ionic state $Cl^+ 3p^4;^1D$. In this calculation we included the $3p^4\,^1D,\epsilon d;^2D$, $3p^4\,^1D,\epsilon d;^2P$, $3p^4\,^1D,\epsilon d;^2S$, and $3p^4\,^1D,\epsilon s;^2D$ channels, using the single-channel values of the dipole transition amplitudes for the $3p^4\,^1D,\epsilon s;^2D$ channel. The $3p^4\,^1D,\epsilon d;^2D$ and $3p^4\,^1D,\epsilon d;^2P$ channels had their coupled-channel K-matrix dipole matrix elements determined in the usual sets of three interacting ^2D channels and two interacting ^2P channels, while the transition amplitudes for the $3p^4\,^1D,\epsilon d;^2S$ channel were determined by coupling the $3p^4\,^1D,\epsilon d;^2S$, $3s\,3p^5;^3P,\epsilon p;^2S$, $3s\,3p^5;^1P,\epsilon p;^2S$, and $3s\,3p^6;^2S$ channels; that is, the four-channel balanced coupling scheme.

The independent- and coupled-channel asymmetry parameters for the $Cl^+ 3p^4;^1S$ multiplet are illustrated in Fig. 8. In this case the β coefficients were evaluated using the $3p^4\,^1S,\epsilon d;^2D$ and $3p^4\,^1S,\epsilon s;^2S$ channels. The channels utilized in determining the channel-interaction dipole matrix elements and transition probabilities for the ^2S channel were the $3p^4\,^1D,\epsilon d;^2S$, $3p^4\,^1S,\epsilon s;^2S$, $3s\,3p^5;^3P,\epsilon p;^2S$, and $3s\,3p^6;^2S$ channels; the transition amplitudes and photoabsorption cross sections for the ^2D channel were found using the three-channel interaction described above in Sec. IV. In this case no correlation was included in the final-state ion. However, the curves obtained for the ^3P and ^1D ionic terms indicate that the primary effect of adding electron correlation into the residual ion, would be to decrease the height of the maxima of the β profiles and to shift them slightly toward lower energies.[10]

Comparison of the HF length (L) and velocity (V) β curves with the corresponding K-matrix channel-interaction profiles in each of the figures clearly exhibits the influence of interchannel interaction. Relative to the single-channel β profiles, coupled-channel β parameters are reduced as the ionic threshold opens, rise more slowly toward lower maxima, decrease from their maxima at about the same rate as the corresponding HF β curves, and pass through zero at a higher photoelectron energy.

At the present time there are no experimental asymmetry parameter measurements available, nor are there any published channel-interaction values, with which to compare the MCHF K-matrix results. The existing theoretical values have been produced by the single-channel open-shell RPAE calculation of Starace and Armstrong,[2] which includes intrachannel interaction but no interchannel-coupling effects, and the recent HF calculation of Manson *et al.*[6]

Our unrelaxed basis evaluations of the uncorrelated HF length spectra (not shown) are in excellent agreement with the frozen-core HF values of Starace and Armstrong[2] for all three $Cl^+ 3p^4$ multiplets, never differing by more than 2%. Moreover, our single-channel β curves do not disagree significantly with their open-shell independent-channel RPAE result, showing divergences of no more than a few percent throughout the photoelectron energy range, for all three residual ion states. More recently, Manson *et al.*[6] have performed a relaxed orbital basis calculation of the length form of the independent-channel β parameters using a single-configuration description of both the initial and final states. Despite our use of an unrelaxed orbital basis, our uncorrelated HF-length β coefficients compare reasonably well with those of Manson *et al.*,[6] differing by no more than about 5%.

VII. CONCLUSIONS

We have evaluated the partial and total cross sections as well as the asymmetry parameters for photoionization of the 3p subshell of neutral chlorine. Electron correlations were considered in both the ground- and final-state channels. Ground-state correlation was included by utilizing the MCHF, while intrachannel final-state electron correlations were introduced through the use of a $MCV^{N-1}(\gamma SL)$ potential. Final-state interchannel correlation effects were investigated by employing K-matrix techniques.

Although all types of electron correlation studied had significant influence on the transition probabilities of the individual final-state channels, the most important contributions were produced by interchannel coupling, particularly for the ^2D and ^2P channels in the vicinity of their ionization thresholds. The K-matrix cross-section curves in these cases were considerably lower than the independent-channel profiles at threshold and had distinct delayed maxima. This contrasted sharply with the single-channel HF curves, which were at their maxima, or nearly so, at threshold. The main effect produced by the other kinds of correlation was to shift the peak of the K-matrix cross sections towards lower photon energies.

One possibly quite significant result obtained in our study was the large mixing weight of single-electron excitations in the multiconfiguration ground and multiconfiguration residual-ion states. As indicated in Tables I—IV, states involving a single $3s \rightarrow \bar{3}d$ excitation are the dominant correlation admixtures in the initial state and in the ^3P and ^1D ionic states. If we consider the effect on the cross sections of the single-electron admixture in the ground state, we find that in each of the ^2D and ^2P channels the transition amplitudes for the larger single-excitation configuration are nearly the same in magnitude as those for all the double-excitation configurations combined. Unfortunately, because of the complicated manner in which these transition amplitudes enter into the calculation of the coupled-channel cross sections, we were unable to determine the importance of the single-electron excitations to the actual final channel-interaction result. These one-electron excitation configurations, though, can have substantial influence on the individual channel transition amplitudes. It should be noted that these single-excited configurations are not included in calculations employing the RPAE method (such as Refs. 2 and 3). Consequently, if these single-electron excitations are important, open-shell versions of the RPAE may have limited applicability.

The total MCHF coupled-channel length and velocity $3p \rightarrow \epsilon d$ cross-section curves are shown in Fig. 5, along with the profiles determined in several other theoretical studies. In the vicinity of the $Cl^+ 3p^4;^1S$ threshold, all of the channel-interaction results are relatively close. From about 0.8 to 1.1 a.u. photon energy, the cross-section spectra break into three groups, with the R-matrix[4] and close-coupling[1] curves forming the highest group, the MCHF and MBPT[5] profiles forming the middle group, and the two open-shell RPAE[2,3] cross-section curves forming the lowest group. There is, therefore, a clustering of total cross sections for calculations employing similar techniques. At photon energies greater than about 1.2 a.u., the

R-matrix curve is substantially higher than that found with any other method (the close-coupling values are given only out to about 1 a.u.). Experimental results in the photon-energy regions 0.8 to 1.1 a.u. or greater than 1.2 a.u. would be quite useful in distinguishing which, if any, of these cross-section curves is valid.

In Sec. IV we discussed the channel-interaction asymmetry parameters for photoionization of the $3p$ subshell of Cl. We found that the disagreement between length and velocity forms of our "best" calculation for β is relatively large, reflecting the well-known fact that the calculation of this quantity is particularly sensitive to the quality of the wave functions used. One reason for this discrepancy may be the way in which $3p \rightarrow \epsilon s$ channels were included in the calculation. That is, in regions in which β is rapidly varying, the cross sections due to $3p \rightarrow \epsilon s$ transitions are relatively large compared to those produced by $3p \rightarrow \epsilon d$ transitions. Unfortunately, we were able to obtain only independent-channel dipole amplitudes for most of these $3p \rightarrow \epsilon s$ transitions, and were thus forced to use values for these dipole matrix elements which are quite possibly not as accurate as those used to describe the $3p \rightarrow \epsilon d$ transitions.

ACKNOWLEDGMENTS

This work was supported in part by the U.S. Department of Energy Contract No. DE-AS02-76ET53006 and National Science Foundation Grant No. PHY-79-21257-01.

*Present address: School of Physics, Georgia Institute of Technology, Atlanta, Georgia 30332.

[1]M. J. Conneely, Ph.D. thesis, London University, 1969 (unpublished); M. J. Conneely, K. Smith, and L. Lipsky, J. Phys. B 3, 493 (1970).

[2]A. F. Starace and L. Armstrong, Jr., Phys. Rev. A 13, 1850 (1976).

[3]N. A. Cherepkov and L. V. Chernysheva, Phys. Lett. 60A, 103 (1977).

[4]M. Lamoureux and F. Combet Farnoux, J. Phys. (Paris) 40, 545 (1979).

[5]E. P. Brown, S. L. Carter, and H. P. Kelly, Phys. Lett. 66A, 290 (1978); Phys. Rev. A 21, 1237 (1980).

[6]S. T. Manson, A. Msezane, A. F. Starace, and S. Shahabi, Phys. Rev. A 20, 1005 (1979).

[7]J. R. Swanson and L. Armstrong, Jr., Phys. Rev. A 15, 661 (1977); 16, 1117 (1977).

[8]M. Ya. Amusia and N. A. Cherepkov, Case Stud. At. Phys. 5, 47 (1975).

[9]P. G. Burke and K. T. Taylor, J. Phys. B 8, 2620 (1975).

[10]W. R. Fielder, Ph.D. thesis, The Johns Hopkins University, 1980 (unpublished).

[11]H. P. Kelly and R. L. Simons, Phys. Rev. Lett. 30, 529 (1973).

[12]C. Froese Fischer, *The Hartree-Fock Method for Atoms* (Wiley, New York, 1977), Chaps. 3 and 4.

[13]C. Froese Fischer, Comput. Phys. Commun. 4, 107 (1972), and private communication.

[14]U. Fano and F. Prats, Proc. Natl. Acad. Sci. (India) A33, 553 (1963).

[15]A. F. Starace (private communication).

[16]R. E. Huffman, J. C. Larrabee, and Y. Tanaka, J. Chem. Phys. 47, 856 (1967).

[17]C. E. Moore, *Ionization Potentials and Ionization Limits Derived from the Analyses of Optical Spectra* (U.S. GPO, Washington, D.C., 1970).

[18]V. L. Jacobs, J. Phys. B 5, 2257 (1972).

[19]R. D. Cowan, L. J. Radziemski, Jr., and V. Kaufman, J. Opt. Soc. Am. 64, 1474 (1974).

[20]U. Fano, Phys. Rev 124, 1866 (1961).

[21]K. Kimura, T. Yamazaki, and Y. Achiba, Chem. Phys. Lett. 58, 104 (1978).